Light Metals 2011 *Edited by: Stephen J. Lindsay*
TMS (The Minerals, Metals & Materials Society), 2011

PARTICULATE EMISSIONS FROM ELECTROLYSIS CELLS

Heiko Gaertner[1], Arne Petter Ratvik[1], Thor Anders Aarhaug[2]

[1]NTNU, Department of Materials Science and Engineering, NO-7491 Trondheim, Norway
[2]SINTEF Materials and Chemistry, NO-7465 Trondheim, Norway

Keywords: Aluminium, Off-gas, Particulates, Fluorides, Emissions

Abstract

In the dry cleaning of the exhaust gas from the aluminium cells impurities are accumulated in the finer fractions of secondary alumina from the dry scrubbers. The present work describes new methods for the determination of dust composition, aiming at increasing the understanding of the effect of cell operation on the amount and the composition of dust in the fume. New and advanced analysis methods are used to characterize a broad specter of emissions. An Electrical Low Pressure Impactor is used to sample and analyze the dust from the cells. The equipment enables real-time particle size distribution analysis of 12 particle classes in the range 30 nm - 10 µm. The size classified samples are analyzed by means of SEM/EDS and XRD to determine the characteristic chemical composition of the different fractions. Understanding the evolution, evaporation, and condensation of particulates in the cell emissions under different operational conditions may facilitate new standards for environmental friendly and energy efficient high amperage electrolysis cells.

Introduction

An understanding of formation, evaporation and condensation of gas compounds in the aluminium electrolysis cell and the off-gas duct system under various operational conditions and current densities are of interest both for setting new standards for environmental friendly production and for efficient operation of high productivity electrolysis cells.

It is commonly accepted that beside the bath chemistry the operational practice has a considerable effect on the gas composition and condensation products in the off gas [1, 2]. Large current density increases may only be realized by increasing the heat losses to maintain the heat balance of the cell. As most of the surplus heat has to be released with the exhaust, it is likely that the particulates formation in the cell will be affected. A higher temperature may affect the cell superstructure and the subsequent gas treatment [3, 4], however, it may be a requirement for economical heat recovery [5, 6]. Also, cost effective CO_2 capture, if developed, requires less draught air to increase the CO_2 concentration, resulting in higher off-gas temperature. Hence, the composition of the finer particulates is of interest, both from a dust recovery perspective and scale buildup in the duct and in heat recovery units.

Fume emitted by aluminum reduction cells with prebaked anodes have been investigated by Less and Waddington [7]. The fume and dust particles sampled under varying operational conditions were examined by chemical analysis, X-ray crystallography, and optical and scanning electron microscopy. Approximately 50 % of the fluoride emissions were in form of particulates. The fine fraction < 2 µm, consisting of condensed fluorides approximating the chiolite composition, contributes about 35 % of the total fluoride emissions. The coarse faction > 6 µm, consisting of alumina, carbon and frozen cryolite droplets, represents about 20 % of the total fluorine emissions. Exact particle size distribution was difficult to determine due to the many different components and the wide range of particle sizes.

In 2000 Hyland, Welch, and Metson [8] reviewed the current knowledge on fluoride and sulfur emissions from aluminum reduction cells. The emissions were classified in two main categories; gaseous emissions as HF, CF_4, C_2F_6, SO_2 and COS and particulates as Na_3AlF_6 (cryolite), $Na_5Al_3F_{14}$ (chiolite), $NaAlF_4$, AlF_3 and CaF_2. The following mechanisms are suggested:

- Vaporization of electrolyte and subsequent condensation as fine particles
- Mechanical entrainment of liquid electrolyte or fines from crust cover material
- HF generation due to reaction of electrolyte with hydrogen from the anodes, vapour or particulates with moisture from air and/or alumina

Based on models assuming that particulates are mainly condensation and hydrolysis products from evaporated $NaAlF_4$, according to Equation 1, different reactions are considered [9,10,11]. The gaseous $NaAlF_4$ may disproportionate to solid chiolite, $Na_5Al_3F_{14}$, and AlF_3 according to Equation 2 and/or undergo hydrolysis as described in Equation 3.

$$Na_3AlF_6(l) = NaAlF_4(g) + 2NaF(l) \quad (1)$$

$$5NaAlF_4(g) = Na_5Al_3F_{14}(g) + 2AlF_3(s) \quad (2)$$

$$3NaAlF4(g;s) + 3H_2O(g) = 6HF(g) + Na_3AlF_6(s) + Al_2O_3(s) \quad (3)$$

Hydrolysis of AlF_3, Na_3AlF_6 and $Na_5Al_3F_{14}$ may occur in contact with moisture in the draught air, Equations 4 and 5.

$$2AlF_3(diss) + 3H_2O(g; diss) = 6HF(g) + Al_2O_3(s; diss) \quad (4)$$

$$3Na_5Al_3F_{14}(g;s) + 6H_2O(g) = 12HF(g) + 5Na_3AlF_6(s) + 2Al_2O_3(s) \quad (5)$$

Höflich *et al.* [12] collected potroom fumes from Søderberg and prebake smelters in a five stage impactor (0.18–0.35 µm, 0.35–0.65 µm, 0.65–1.2 µm, 1.2– 3.5 µm and 3.5–10 µm). The electron microscopy approach to determine the particle distribution substantially underestimates the particle concentrations in the size range below 300 nm as shown elsewhere [13]. With 45–65 % particles containing O, F, Na and Al, a mixture of aluminium oxide and cryolite are most abundant in the potroom air. The ultrafine particles are considered to be condensation and hydrolysis products of vapor compounds from the electrolyte.

Large carbon particles (up to a few μm) are most likely entrained dust from the anodes. Due to the complex chemical composition, it is assumed that agglomerates contain additional phases as aluminium oxides, cryolite, silicates and sulfides/sulfates. The authors also noticed needle-like particles.

Experimental

An Electrical Low Pressure Impactor, DEKATI ELPI™, is used for real-time sampling of 12 particle classes in the size range 7 nm – 10 μm. The operating principle can be divided into three parts; particle charging, size classification in a cascade impactor, and electrical detection with electrometers. The particle collection on each collector plate stage is dependent on the aerodynamic size of the particles. Measured current signals are converted to particle number and size distributions. The size classified samples over the operational range of the impactor instrument is given in Table I.

Table I. Size classification and mass characteristics of the Dekati ELPI™ impactor 10 lpm (without dilution). Inlet pressure 1013.3 mbar, temperature 21.6 °C.

Stage	D50	Di	Number ($1/cm^3$)		Mass ($\mu g/m^3$)	
	(μm)	(μm)	min	max	min	max
13	9.85					
12	6.64	6.25	0.10	2.0E+04	31	8300
11	3.97	3.07	0.10	2.0E+04	10	2700
10	2.38	1.95	0.17	4.5E+04	3	810
9	1.59	1.22	0.33	8.8E+04	1.4	370
8	0.942	0.76	0.60	1.6E+05	0.7	180
7	0.609	0.48	0.11	2.9E+05	0.03	80
6	0.378	0.31	2.0	9.8E+00	0.1	40
5	0.259	0.19	3.7	9.8E+00	0.07	18
4	0.153	0.11	6.0	1.7E+06	0.03	8
3	0.0908	0.70	12	3.1E+06	0.02	4
2	0.0541	0.04	23	6.1E+06	0.006	1.7
1	0.0279	0.02	50	1.4E+07	0.002	0.5
Filter	0.07	0.014	250	6.9E+07	0.0004	0.11

The experimental setup for the impactor is shown in Figure 1.

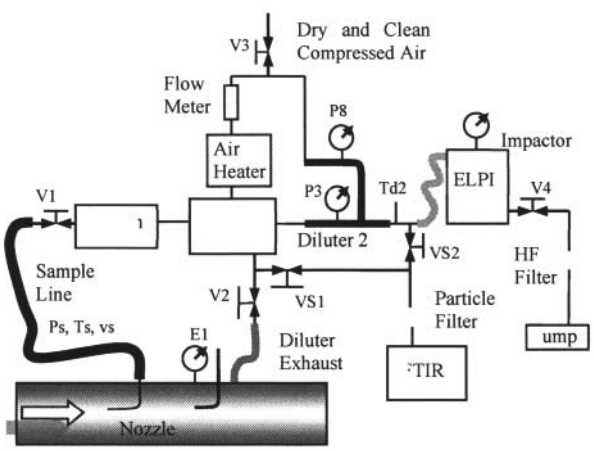

Figure 1: Sketch of experimental setup for sampling of particulate emissions.

The equipment consists of a heated sampling and dilution line (Dekati ejector diluter and DAD-100 axial diluter). A cyclone collects the coarse dust particles before the diluter. The residual fine particles, D50 < 10 μm is feed to the impactor with a flow of 10 l/minute. Dilution ratios were determined with a Portea 204M/C FTIR by comparing concentration changes in tracer gas before and after the dilution. The Dekati ELPIVI 4.0 software was used to compute the particle numbers. Particles on impactor substrates were dried at 120 °C for 24 hours before weighing and further analysis.

A Testo 435, Pitot tube and Fluke Thermologger with K-type thermocouple were used to determine the duct gas velocity and temperature in the duct.

An Actaris gas meter type G4 (0.04–6 m^3/h) was used to monitor the gas flow when dust samples were collected on filters. The dust samples were dried at 160 °C until constant weight was achieved.

A LVSEM type Hitachi S-3400N and a FESEM type Zeiss Ultra 55 Limited Edition were used to perform optical and X-ray energy dispersive spectrometer (EDS) analysis of the samples. Non-conducting samples were not coated. To prevent accumulation of electrostatic charge the Hitachi S-3400N was operated in low vacuum mode at 70 Pa using the BSE (backscatter electron) detector. To achieve high resolution micrographs, the FESEM type Zeiss Ultra 55 was operated in the low voltage SE mode at 2 kV to reach a dynamic charge balance, as described by Yu et al. [14].

A Bruker AXS D8-Focus X-ray powder diffraction (XRD) and EVA 15.0.0.0 analysis software were used to identify different crystalline phases in the filter dust samples.

The laser diffraction analysis of filter samples were performed with a Mastersizer 2000 APA200 (Malvern Instruments Ltd) with a size range of 0.02 to 2000 μm. Powder from filter samples were dispersed in water under ultrasonic agitation for 90 seconds before passing the laser beam in the closed Hydro MU dispersion loop. Particle distribution was converted from volume to number distribution.

Results and Discussion

Impactor

Various impactor substrates are used to accommodate different objectives. Samples deposited on aluminum foils are used for image analysis, while polycarbonate substrates are used for chemical analysis. On aluminium, silver and polycarbonate substrates, we typically observe a shift in the impactor recordings during the initial period as shown in Figure 2.

For the substrates capturing the coarser particles, this effect may be due to particles bouncing off the substrates or smaller particles released from agglomerates hitting the plates. As the opposite effect is observed for the substrates capturing the finer particles the breakup of agglomerates seems to be the most likely cause. The effect on calculated mass concentrations due to the initial variations is illustrated in Figure 3. Using sintered substrates with an oil film reduces this effect significantly. However, these substrates are not suited for chemical analysis as the oil film interferes with subsequent analysis.

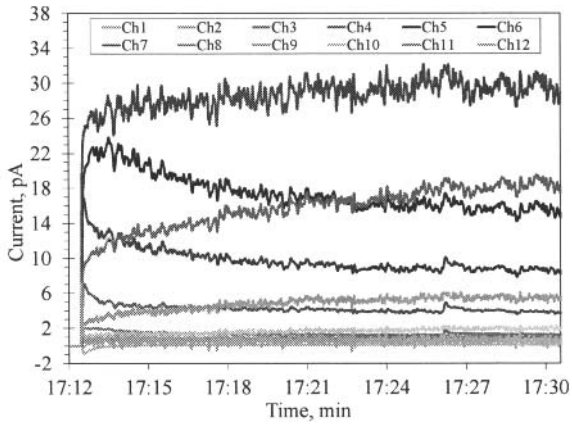

Figure 2. Impactor recordings of particulates in the raw gas using aluminium substrates. Measured current [pA] is proportional to the number of particles collected on each impactor stage.

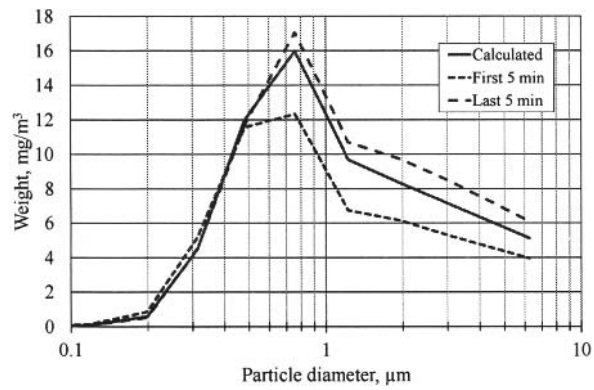

Figure 3: Effect of initial and final period versus total calculation of particles hitting the impactor plates.

Compared to electron microscopy data published by Höflich [9], a significant higher number of smaller particles than 0.5 µm are observed with the present impactor method, making the method well suited for extracting on-line information on the state of the particulates in the off-gas from the cell and in the potroom air.

Scrubber

To obtain recordings of dry scrubber performance, gas samples for one filter line were drawn from the stack between the dry and wet scrubbers. For comparison, also ambient air at the same location is measured. The results, calculated by Dekati ELPI software assuming particle density equal 1 g/cm^3, are shown in Figure 4.

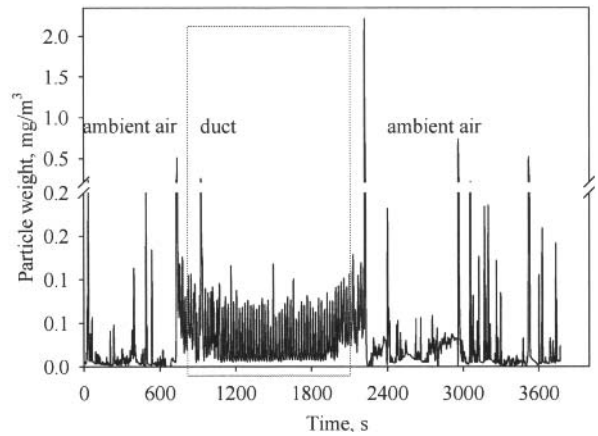

Figure 4. The particle weight as function of time sampled between the dry and wet scrubbers and in ambient air. Weights are calculated based on assumed particle density of 1 g/cm^3. Marked window is shown in Figure 5.

Compared to the ambient air at the sampling location, the concentration in the duct for the different particle classes varies from 0.4 to 4.7 times the mg/m^3 concentrations of the ambient air. Wind gusts gave a temporary and significant increase in recorded particle concentrations at the sampling location, especially noticeable for the finer fractions below 1 µm. Average particle concentrations are given in Table II.

Table II. Calculated weight on the impactor plates after the dry scrubber and ambient air for the given average particle sizes.

Di µm	Duct µg/m^3	Air µg/m^3	Ratio (Duct/Air)
0.0279	0.044	0.108	0.41
0.0541	0.175	0.384	0.46
0.0908	0.48	1.10	0.44
0.153	1.22	2.62	0.46
0.259	4.32	4.45	0.97
0.378	17.4	4.28	4.07
0.609	12.7	2.74	4.66
0.942	5.11	1.39	3.67
1.59	4.76	1.48	3.21
2.38	7.68	3.18	2.41
6.64	3.30	4.07	0.81
9.85	66.1	36.6	1.81
Concentration	37.2	19.8	1.88
Number of data points	1441	2211	
Density g/cm^3	1	1	

The measured period after the scrubber is extracted to Figure 5. Cyclic changes in the particle recordings are in phase with the filter-bag regeneration pulses. The leakage through the filter varies between 0.01 to 0.07 mg/m^3 during each cycle. The coarser particles have sharper peaks than the finer particles as shown in Figure 6. This is expected as the new filter cake build-up after cleaning initially captures coarser particles more effectively than finer particles. The measurements show that it is possible to determine the effect of the cleaning cycle and the state of the filter bags. Although not investigated in the present work, it is believed that the method is well suited for improving bag performance and

determining optimal conditions for efficient cleaning with lowest possible dust leakage through the filter bags.

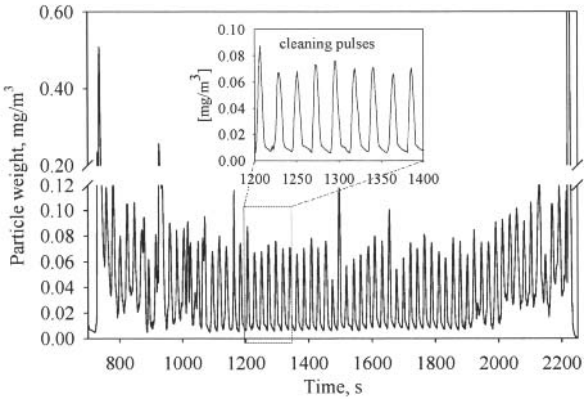

Figure 5. Particles in the gas duct after the dry scrubber.

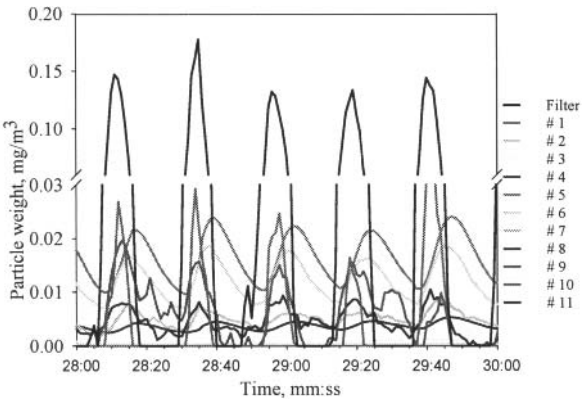

Figure 6. Particle distribution on the various impactor plates over some of the bag cleaning periods; particle sizes corresponding to the impactor plates can be read from Table II.

Duct

Results from sampling of the finer fractions of the raw gas in the duct at two plants are presented in Figure 7. Subject to normal operations, the distribution of finer particles is comparable between the plants.

In Figure 8, the calculated weight distribution is compared with gravimetric determination of each individual impactor plate. The calculated values are slightly shifted to higher values. This may be due to variations in real density of the particles as the impactor software assumes a constant density, in this case set to 1 g/cm^3, or errors due to the bouncing effect. For all substrate types the particle classes with 0.032 µm ≤ Di ≤ 3.078 µm the computed values differ approximately 0.7 to 2.4 times from the concentrations determined by weighing. This will be addressed in future work, e.g. by using longer sampling times. Due to a high standard deviation of the weight of the impactor plates for the finest particles, the values of the finer fractions must be interpreted with caution.

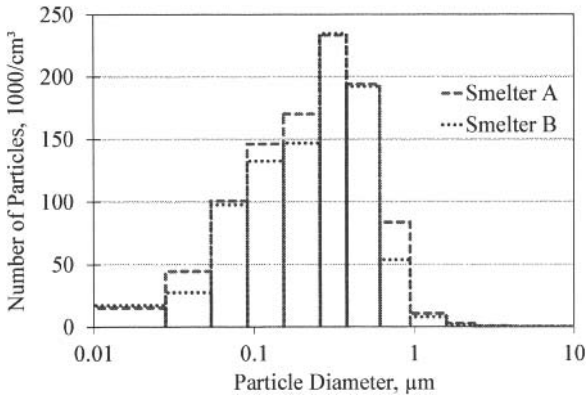

Figure 7. Distribution of finer particles in the raw gas sampled in the main duct of a production line before the dry scrubber at two different smelters (as recorded on substrates).

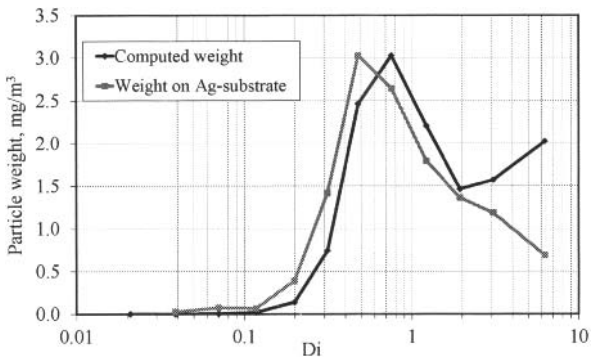

Figure 8. Gravimetric analysis of particulates collected on aluminium or polycarbonate substrates compared to computed weight based on measured number of particles with assumed density of 1 g/cm^3.

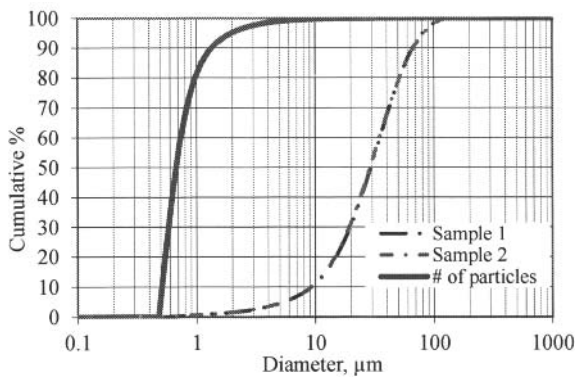

Figure 9. Cumulative particle distribution determined by Malvern Mastersizer.

The number concentration computed by the impactor software given in Figure 6 is compared to filter samples analyzed using a Malvern Mastersizer, Figure 13. The Malvern does not account for a significant number of the particles with median diameter < 0.5 µm. This is most likely due to agglomeration of the particles on the filter, which is not dissolved in the water during ultrasonic

agitation, indicating that current impactor measurements are better suited for the determination of the fines in the raw gas from the electrolysis cells.

Particulates

Scanning electron microscopy images, Figure 10, 11 and 12, show that the dust particles adopts numerous shapes, all from discrete spherical droplets, platelets and hexagonally shaped primary particles to agglomerates and particles embedded in a composite matrix of oblong or needle shaped fibrous framework with alumina, cryolite and sodium aluminum fluoride. Typically, many of the fibers seem to be formed at an early stage acting as condensation sites for the vapour phase forming knobbly or grapelike droplets and smaller particles.

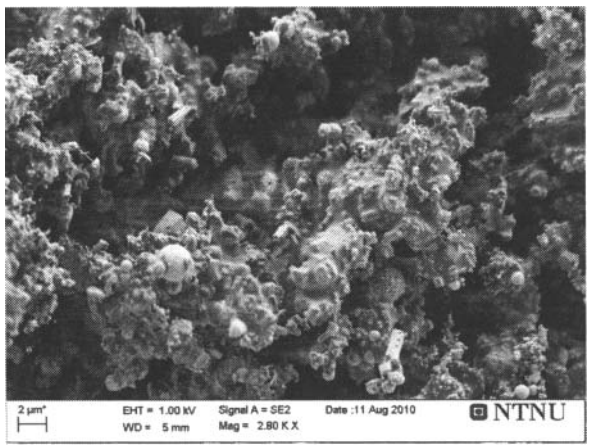

Figure 10. Sponge-like structure of samples with D50 = 1.590 µm.

On substrates with Di = 2.39 µm individual particles can quite easily be identified while particulates on the impactor stages with Di < 1.59 µm the agglomerates seem to grow together to a fabric framework. This is probably due to higher surface forces of the smaller particles, resulting in particles growing together.

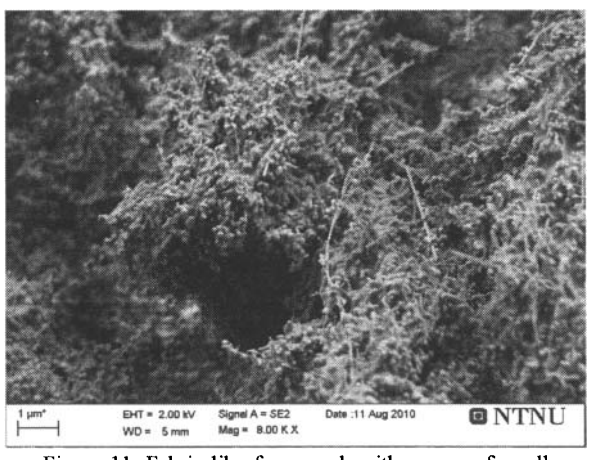

Figure 11. Fabric like framework with grapes of smaller particulates attached to oblong particles/fibers of samples with D50 = 0.259 microns.

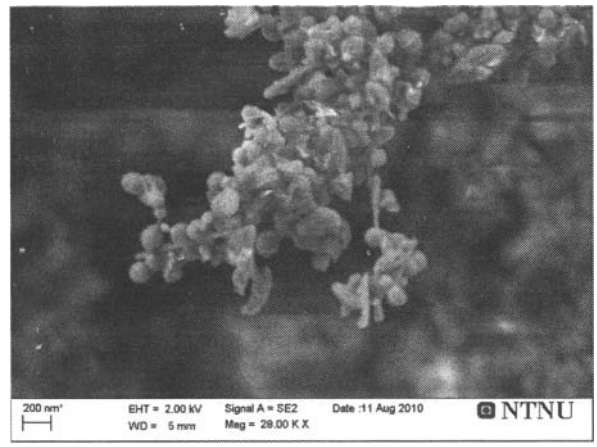

Figure 12. Grapelike condensate structure on fibers.

Based on a qualitative chemical analysis the most dominant particle group contains sodium, aluminum, oxygen and fluorine. For the particle size ranges with Di equal 60.9 nm, 942 nm, 1.59 µm and 2.38 µm, respectively, the atomic ratio of the elements are close to Na:Al:O:F = 1:1.1:2.2:5.6.

In the pictures taken with help of the BSE detector, Figure 12, heavier elements appear brighter and stand out from the lighter surroundings. The BSE analysis shows a large variety of morphologies of coarse particles and agglomerates. Ni, Fe and S containing particles are identified due to their very bright appearance. Often the brighter particles are located with the carbon particles. Possibly, the heavier elements are abrasion products.

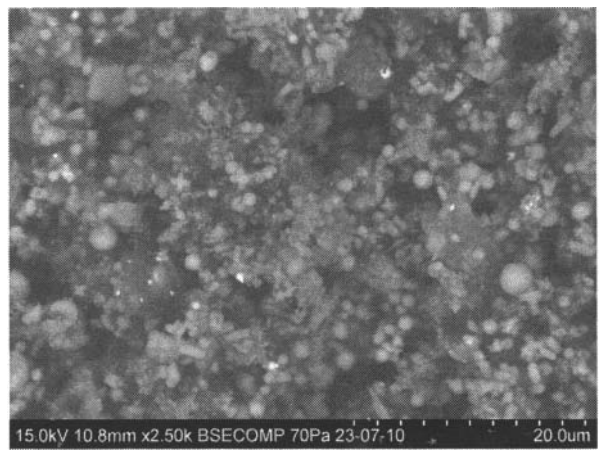

Figure 12. Backscatter image showing discrete particles and complex agglomerates of droplets. Heavier elements appear brighter than binder matrix.

The XRD analysis of filter samples shows the dominant phases to be cryolite Na_3AlF_6, chiolite ($Na_5Al_3F_{14}$) and corundum (Al_2O_3). Sulfur may be present in the form of sulfates attached to sodium and/or alumina as millosevichite, $Al_2(SO_4)_3$, or matteuccite, $NaHSO_4 \cdot H_2O$, which is identified in the XRD pattern. Large carbon rich agglomerates (up to a few µm) are observed, which is most likely entrained dust from the anodes. Soot particles are abundant in the fractions with particle sizes above 1.59 µm. For

the finer particulates with D50 below 1.59 μm, sampled on silver substrates, the XRD shows that the dominating compound is $NaAlF_4$. The XRD identification of $NaAlF_4$ is in accordance with Gylseth *et al.* [15] and Heiberg *et al.* [16] who reported fibrous $NaAlF_4$ in the potroom air. Also Kirik and Zaitseva [17] report the formation of metastable fibrous crystals and colorless $NaAlF_4$ powder by condensing vapors arising from chiolite heated to 800 °C. The condensed $NaAlF_4$ was stable up to 390-400 °C before disproportionating exothermally into solid $Na_5Al_3F_{14}$ and AlF_3 and into solid Na_3AlF_6 and gaseous $NaAlF_4$ at higher temperatures. The high amount of $NaAlF_4$ on the substrates with the finer particles indicates that most of the finer particulates are rapidly quenched to low temperatures by the draught air in the cell.

Dando and Lindsay [18] found that hard gray scale (HGS) in dry scrubbing consisted of an amorphous reaction product formed from the attrition-induced reaction of bath superfines, alumina fines and water. HGS could be artificially created by co-grinding these three components. It is postulated that the energy release by "new alumina surface" re-hydration is the principal energy driver. If any of the three ingredients was left out, scale was not formed.

The present work indicates that the particulate fines in the raw gas may possess fouling properties. Chemical composition and origin of different particle size classes will be studied further and compared to deposition mechanisms in heat exchangers to identify particle groups having an effect on both the growth and removal of depositions.

Conclusions and Further Work

On-line sampling and monitoring of changes in composition of particulate fines in the off-gas from aluminium cells are established and will be used in future work to compare the effects of various operational parameters.

Larger numbers of particles in the sub-micron range are measured with the impactor equipment than previously reported. The SEM pictures of the size classified particulates reveal a change in agglomerate morphology for the different particle size classes. Further work will also focus more on formation mechanisms of the observed compounds and agglomeration products. Also, samples will be collected on silver substrates for better EDS and TEM analysis of the different particle size classes.

Acknowledgment

This study is a part of the ROMA research project with financial support from the Research Council of Norway and Norwegian aluminum and metallurgical industry. An essential part of this research is conducted as measurement campaign at industrial cells. We appreciate the support by operators at Alcoa Mosjøen and Hydro Sunndal.

References

1. W. Wahnsiedler, R. Danchik, D. Backenstose, W. Haupin, and J. Colpitts, "Factors affecting fluoride evolution from Hall-Heroult smelting cells," *Light Metals* 1978, pp. 407–421
2. C.N Cochran, W.C. Sleppy and W.B. Frank, "Fumes in Aluminium Smelting: Chemistry of Evolution and Recovery," *Journal of Metals*, Sep 1970, pp. 54-57
3. A. Sørhuus and G. Wedde, "Pot gas heat recovery and emission control," *Light Metals* 2009, pp. 281-286.
4. S.J. Linday, and N.R. Dondo, "Dry Scrubbing for Modern Pre-Bake Cells," *Light Metals* 2009, pp 275-280
5. A. Solheim, B. Moxnes, K. Vamraak and E. Haugland, "Energy recovery and amperage increase in aluminium cells by active cooling in the anode yokes," *Light Metals* 2009, pp. 1091-1096
6. M. Fleer, O.-A. Lorentsen, W. Harvey, H. Palsson and G. Sævarsdottir, "Heat recovery from exhaust gas of aluminium reduction cells," *Light Metals* 2010, pp. 243-248
7. L. Less and J. Waddington, "The characterization of aluminium reduction cell fume", *Light Metals* 1971, pp. 499–508
8. M. Hyland, B.Welch and J. Metson, "Changing knowledge and practices towards minimising fluoride and sulphur emissions from aluminium reduction cells," *Light Metals* 2000, pp. 333–338
9. W. Haupin, "Mathematical model of fluoride evolution from Hall-Heroult cells," *Light Metals* 1984, pp. 1429–1439
10. W. Haupin and H. Kvande, "Mathematical model of fluorine evolution from Hall-Heroult cells", *Light Metals* 1993, pp. 257–263
11. B. V. L'vov, L. K. Polzik, S. Weinbruch, D. G. Ellingsen, and Y. Thomassen, "Theoretical aspects of fluoride air contaminant formation in aluminium smelter potrooms", *J. Environ. Monit.*, 7(2005)425–430
12. B.L.W. Höflich, S. Weinbruch, R. Theissmann, H. Gorzawski, M. Ebert, H.M. Ortner, A. Skogstad, D.G.Ellingsen, P.A. Drabløs and Y. Thomassen, "Characterization of individual aerosol particles in workroom air of aluminium smelter potrooms," *J. Environ. Monit.*, 7(2005)419–424
13. M. Ebert, S. Weinbruch, A. Rausch, G. Gorzawski, P. Hoffmann, H. Wex and G. Helas, "Complex refractive index of aerosols during lace 98 as derived from the analysis of individual particles," *Journal of geophysical research: Atmospheres*, vol. 107, NO. D21, 8121, doi:10.1029/2000JD000195, pp. LAC 3, 1–15, September 2002
14. Y.D. Yu, M.P. Raanes and J. Hjelen, "Characterization of nonconductive polymer materials using FESEM," in *Proceedings of the 17th International Microscopy Congress (IMC17)*, Rio de Janeiro, Brazil, 19-24 September 2010
15. B. Gylseth, O. Bjørseth, Ø. Dugstad and J. Gjønnes, "Occurrence of fibrous sodium aluminumtetrafluoride particles in potrooms of the primary aluminum industry," *Scand. J. Work Environ. Health*, 10(6)(1984)189–195
16. A.B. Heiberg, G. Wedde, O.K. Bøckman and S.O. Strømmen, "Pot gas fume as a source of HF emissions from aluminium smelters – Laboratory and field investigations," *Light Metals* 1999, p 255-261
17. S.D. Kirik and J.N. Zaitseva, "$NaAlF_4$: Preparation, crystal structure and thermal stability", *Journal of Solid State Chemistry*, 183(2010)431–436
18. N.R. Dando and S.J. Lindsay, "Hard Gray Scale," *Light Metals* 2008, pp. 227- 232